Journal of Marine Research, 55, 293–320, 1997

Influences of river discharge on biological production in the inner shelf: A coupled biological and physical model of the Louisiana-Texas Shelf

by Changsheng Chen[1], Denis A. Wiesenburg[2], and Liusen Xie[1]

ABSTRACT

A coupled biological and physical model was applied to study the influence of river discharge on biological variability on the Louisiana-Texas (LATEX) continental shelf. The physical part included a primitive-equation turbulent closure model, and the biological part was a simple phytoplankton (P), zooplankton (Z), and nutrient (N) model. The model was forced by freshwater discharge from the river and ran prognostically under initial conditions of springtime water stratification and a steady-state solution of the P-Z-N model with no horizontal dependence. A nutrient source was included at the mouth of the river. The model predicted a well-defined density frontal zone on the inner shelf. The biological field showed a region of high phytoplankton biomass in the whole water column near the coast and a moderately high biomass patch in the upper 10 m at the outer edge of the frontal zone. A high concentration dome of nutrients was found near the bottom within the frontal zone. New production of nutrients was high throughout the whole water column near the coast and in the upper 10 m at the outer edge of the density front, but lower in the frontal zone. The model results were in reasonable agreement with observational data taken from a May 1993 interdisciplinary survey on the LATEX shelf.

Cross-shelf distribution of biological production varied significantly with direction of wind stress but not with the diurnal tide. The model results suggested that the bottom-rich nutrient distribution within the frontal zone was caused by the interaction of physical and biological processes. Physical processes caused the formation of an area of high nutrient concentration in the weak current region within the frontal zone. Subsequent biological processes limited the increase of nutrients in the upper euphotic zone and hence led to the bottom-rich nutrient pattern.

1. Introduction

The Louisiana-Texas (LATEX) continental shelf in the Gulf of Mexico is well known for high biological productivity associated with this unique physical environment (Riley, 1937; Sklar and Turner, 1981). Primary production on the LATEX shelf has been observed to be closely tied to the seasonal discharge of the nutrient-rich freshwater from the

1. Department of Marine Sciences, The University of Georgia, Athens, Georgia 30602-2206, U.S.A. E-mail: chen@whale.marsci.uga.edu.

2. Institute of Marine Sciences, University of Southern Mississippi, Stennis Space Center, Mississippi, 39529, U.S.A.

Mississippi and Atchafalaya River (MAR) system at the coast, upwelling associated with the Loop Current eddies at the shelf break, and local wind and tidal mixing (Lohrenz *et al.*, 1990; Bierman *et al.*, 1994; Sahl *et al.*, 1993; Neuhard, 1994). An interdisciplinary field program conducted during May 1993 over the LATEX shelf showed a high level of phytoplankton biomass in the inner shelf, which was strongly linked to the unusually large freshwater discharge from the MAR system (Figs. 1 and 2). The average freshwater flux during May 1993 was about 32,900 m^3/s at the Mississippi River and 14,700 m^3/s at the Atchafalaya River, which was about 10,000 m^3/s (Mississippi River) and 6,000 m^3/s (Atchafalaya River) larger than the May discharges averaged over the sixty-two year records from 1930 to 1992 (Wiesenburg *et al.*, 1994; Dinnel and Wiseman, 1986).

Hydrographic data, taken from the May 1993 interdisciplinary survey, has shown a relatively strong, low-salinity (or density) surface-bottom frontal zone near the 20 to 40-m isobaths (Figs. 1 and 2). In addition to a high concentration of nitrate and chlorophyll *a* near the coast, nitrate concentrations showed a distinct maximum value at the bottom, within the low-salinity front that was located at the 20 to 30-m isobaths on Sec. 1 and at the 20 to 40-m isobaths on Sec. 2 (Fig. 2). This bottom-rich nitrate pattern extended offshore to a region of deeper than 60 m on Sec. 1, the section between the Mississippi and Atchafalaya rivers. However, on Sec. 2 west of the Atchafalaya River, the nitrate maximum dome seemed to be isolated from the outer shelf nitrate source.

High nitrate concentrations, which were observed near the bottom on the middle shelf, may result from the interaction of biological and physical processes associated with a low-salinity front. In terms of biological processes, benthic regeneration may become important in the middle shelf where there is no significant input of riverine nutrients (Flint and Kamykowski, 1984; Rowe *et al.*, 1975). The possible presence of bottom nepheloid layers on the middle shelf, as a consequence of suspension of sediment due to tidal and strong wind mixing, would supply nutrients from benthic regeneration and zooplankton excretion near the bottom (Shiderler, 1975; Kamykowski and Bird, 1981; Neuhard, 1994). Since the dome of maximum nitrate was observed near the bottom within the low-salinity front, physical processes associated with the front formation and cross-front secondary circulation may become critically important in the generation of the bottom-rich nitrate pattern on the middle shelf. However, the detailed relationship of such a biological pattern with the dynamics of the low-salinity front on the LATEX shelf has not been previously investigated.

To examine the biological and physical mechanisms controlling primary production and plankton patches near the coast and within the low-salinity frontal zone in the inner LATEX shelf, we have applied a fully coupled physical and biological model to the LATEX shelf. This coupled model was developed by Franks and Chen (1996). To better understand the basic dynamic processes that control the cross-shelf distribution of biological production, we have simplified our modeling experiments to a two-dimensional (so-called 2-D) problem. The model considered a cross-shelf slice of the LATEX shelf in which the along-shelf variation for all independent variables was ignored. Although the

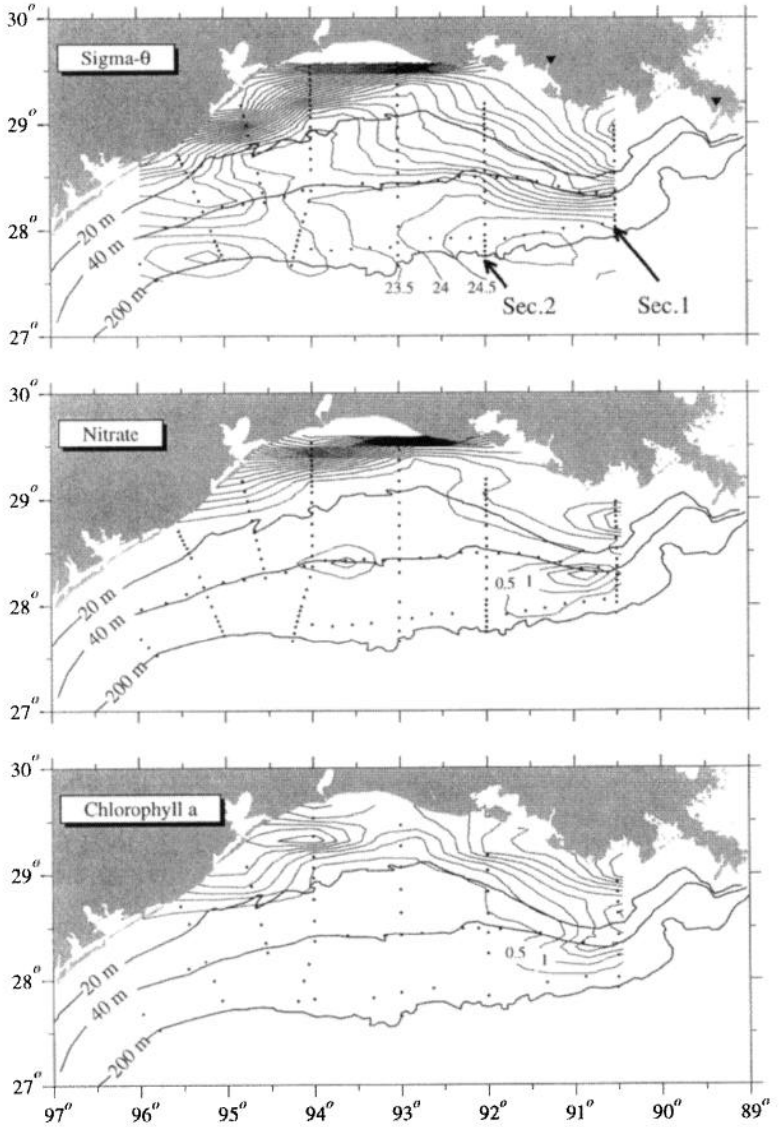

Figure 1. Distributions of the surface density (σ_θ: kg/m^3), nitrate (μmole N l^{-1}), and chlorophyll *a* (μmole N l^{-1}) during April 26–May 10 1993. Solid filled circles represent the measurement stations. Filled downtriangles indicate the locations of the rivers.

contribution of along-isobath advection from the Mississippi River was ignored in this simple model, the model results showed a reasonable agreement with observed biological data and have given us insight into the mechanisms supporting primary production and phytoplankton distributions over the inner LATEX shelf.

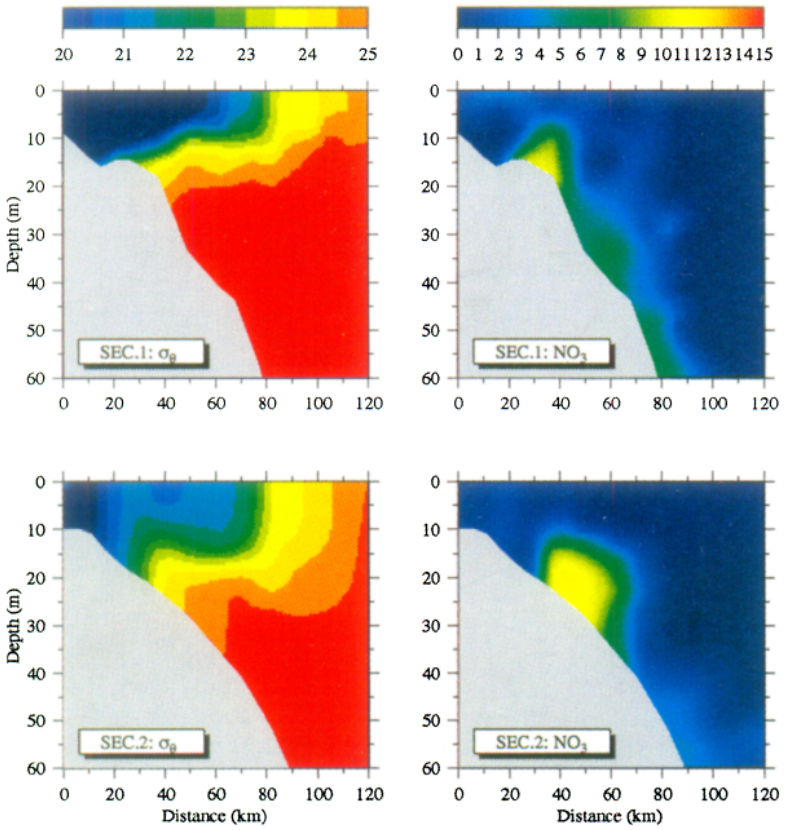

Figure 2. Cross-shelf distributions of the density (σ_θ: kg/m^3) and nitrate (μmole N l^{-1}) on Sec. 1 and Sec. 2 shown in Figure 1.

2. Coupled physical and biological model

a. Physical model

The physical model used in this study is a modified version of the three-dimensional (so-called 3-D) coastal ocean circulation model developed originally by Blumberg and Mellor (1987). This model incorporates the Mellor and Yamada (1974 and 1982) level 2.5 turbulent closure scheme to provide a realistic parameterization of vertical mixing that has been found critically important for coastal mixing and cross-shelf circulation (Wright and Loder, 1985; Chen and Beardsley, 1995; Chen *et al.,* 1995). A free surface is coupled with this model, which allows simulation of surface wave propagation such as tides and long gravity waves. Time variable river/dam and onshore intake/outflow discharges also are included in the model for the study of buoyancy-driven circulations caused by river discharges.

A σ-coordinate transformation is used in the vertical and a curvilinear coordinate system in the horizontal, which allow a smooth representation of irregularly variable bottom

topography and real coastal geometry. To improve the computational efficiency, the model incorporates a semi-implicit scheme for time-stepping of the barotropic mode (Casulli, 1990). A modification of the stability functions made by Galperin *et al.* (1988) was recently included in the Blumberg and Mellor model. An updated version of this model was described in detail in Blumberg (1994) and Chen and Beardsley (1995). A brief description of the 2-D version of this model is given here to provide a systematic understanding of how biological and physical models were coupled.

The model consists of momentum, continuity, temperature, salinity, and density equations:

$$\frac{\partial u}{\partial t} + u\frac{\partial u}{\partial x} + w\frac{\partial u}{\partial z} - fv = -\frac{1}{\rho_o}\frac{\partial p}{\partial x} + \frac{\partial}{\partial z}\left(K_m\frac{\partial u}{\partial z}\right) + F_u \tag{2.1}$$

$$\frac{\partial v}{\partial t} + u\frac{\partial v}{\partial x} + w\frac{\partial v}{\partial z} + fu = \frac{\partial}{\partial z}\left(K_m\frac{\partial v}{\partial z}\right) + F_v \tag{2.2}$$

$$\frac{\partial p}{\partial z} = -\rho g' \tag{2.3}$$

$$\frac{\partial u}{\partial x} + \frac{\partial w}{\partial z} = 0 \tag{2.4}$$

$$\frac{\partial \theta}{\partial t} + u\frac{\partial \theta}{\partial x} + w\frac{\partial \theta}{\partial z} = \frac{\partial}{\partial z}\left(K_h\frac{\partial \theta}{\partial z}\right) + F_\theta \tag{2.5}$$

$$\frac{\partial s}{\partial t} + u\frac{\partial s}{\partial x} + w\frac{\partial s}{\partial z} = \frac{\partial}{\partial z}\left(K_h\frac{\partial s}{\partial z}\right) + F_s \tag{2.6}$$

$$\rho_{\text{total}} = \rho_{\text{total}}(\theta, s) \tag{2.7}$$

where x, y, and z are cross-shelf, along-shelf, and vertical axes of the Cartesian coordinate (Fig. 3); u, v, and w the x, y, z velocity components; θ the potential temperature; s the salinity; p the pressure; f the Coriolis parameter; g' the gravitational acceleration; K_m the vertical eddy viscosity coefficient; and K_h the thermal vertical eddy friction coefficient. F_u, F_v, and F_θ represent the horizontal momentum and thermal diffusion terms. ρ and ρ_o are the perturbation and reference density, which satisfy

$$\rho_{\text{total}} = \rho + \rho_o \tag{2.8}$$

The cross-shelf stream function is defined as

$$\psi = -\int_{-H(x)}^{z} u\,dz \tag{2.9}$$

where $H(x)$ is the water depth. The vertical eddy viscosity was calculated using the second-order turbulent closure scheme (level 2.5) developed by Mellor and Yamada (1974,

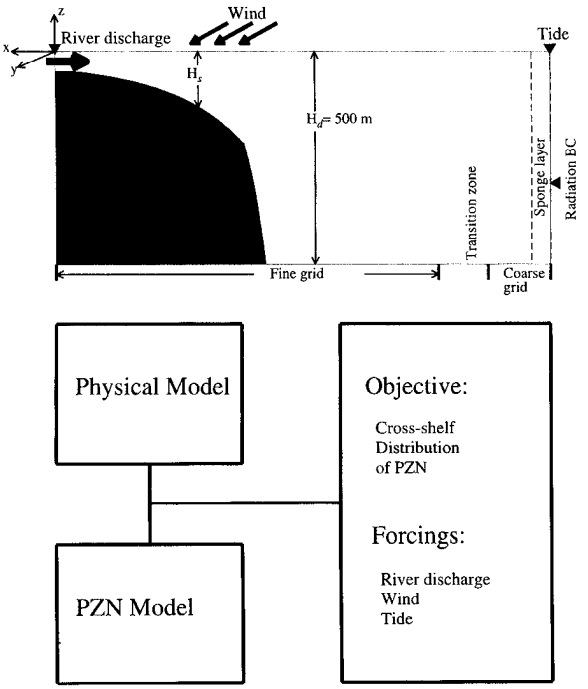

Figure 3. Schematic of the design and objective of the numerical simulations on the inner LATEX shelf.

1982). Under the boundary layer approximation, where the shear production of turbulent energy can be neglected except in the vertical, the eddy viscosity can be calculated through the closure turbulent kinetic energy and turbulent macroscale equations. A detailed description of the turbulent closure scheme, which was used in our 2-D model, can be seen in Chen and Beardsley (1995).

b. Biological model

The biological model is a simple nutrient (N), phytoplankton (P) and zooplankton (Z) model (Franks *et al.*, 1986) in which dissolved nutrients are taken up by the phytoplankton following Michaelis-Menten kinetics, and phytoplankton are grazed by zooplankton with an Ivlev functional response:

$$\frac{\partial P}{\partial t} + u\frac{\partial P}{\partial x} + w\frac{\partial P}{\partial z} = \frac{V_m N}{k_s + N} f(I_o)P - ZR_m(1 - e^{-\lambda P}) - \epsilon P + \frac{\partial}{\partial z}\left(K_p \frac{\partial P}{\partial z}\right) \tag{2.10}$$

$$\frac{\partial Z}{\partial t} + u\frac{\partial Z}{\partial x} + w\frac{\partial Z}{\partial z} = (1 - \gamma)ZR_m(1 - e^{-\lambda P}) - gZ + \frac{\partial}{\partial z}\left(K_z \frac{\partial Z}{\partial z}\right) \tag{2.11}$$

$$\frac{\partial N}{\partial t} + u\frac{\partial N}{\partial x} + w\frac{\partial N}{\partial z}$$

$$= -\frac{V_m N}{k_s + N} f(I_o)P + \gamma Z R_m(1 - e^{-\lambda P}) + \epsilon P + gZ + \frac{\partial}{\partial z}\left(K_p \frac{\partial N}{\partial z}\right) \quad (2.12)$$

where

$$N + P + Z = N_T, \quad (2.13)$$

and N_T is the total amount of nutrients (μmole N l^{-1}), V_m the maximum phytoplankton growth rate; k_s the half-saturation constant for phytoplankton growth, R_m the maximum grazing rate of phytoplankton by zooplankton, λ the grazing efficiency of phytoplankton by zooplankton, γ the fraction of ingested phytoplankton unassimilated by zooplankton, ϵ the phytoplankton death rate, g the zooplankton death rate. The phytoplankton depends on incident irradiance I_o though the function $f(I_o)$ that we have taken to be linear:

$$f(I_o) = I_o e^{-k_{ext}z}, \quad (2.14)$$

where k_{ext} is the diffuse attenuation coefficient for irradiance. K_N, K_P, and K_Z are the vertical eddy diffusion coefficients of nutrients, phytoplankton, and zooplankton, respectively. For simplification, we assumed that mixing of biological variables was controlled by physical processes, i.e., $K_N = K_P = K_Z = K_m$. The detailed description for coupling of physical and biological models can be seen in Franks and Chen (1996).

c. Boundary conditions

In the absence of surface and bottom heat fluxes, the surface and bottom boundary conditions are

$$\left.\begin{aligned} &\frac{\partial \theta}{\partial z} = \frac{\partial s}{\partial z} = \frac{\partial P}{\partial z} = \frac{\partial Z}{\partial z} = \frac{\partial N}{\partial z} = 0, \quad w = \frac{\partial \zeta}{\partial t} + u\frac{\partial \zeta}{\partial x} \\ &K_m\left(\frac{\partial u}{\partial z}, \frac{\partial v}{\partial z}\right) = (\tau_{sx}, \tau_{sy})/\rho \end{aligned}\right\} \quad \text{at } z = \zeta(t, x) \quad (2.15)$$

and

$$\left.\begin{aligned} &\frac{\partial \theta}{\partial z} = \frac{\partial s}{\partial z} = \frac{\partial P}{\partial z} = \frac{\partial Z}{\partial z} = \frac{\partial N}{\partial z} = 0, \quad w = -u\frac{\partial H}{\partial x} \\ &K_m\left(\frac{\partial u}{\partial z}, \frac{\partial v}{\partial z}\right) = (\tau_{bx}, \tau_{by})/\rho \end{aligned}\right\} \quad \text{at } z = -H(x) \quad (2.16)$$

where $(\tau_{sx}, \tau_{sy}) = C_d\sqrt{u_s^2 + v_s^2}(u_s, v_s)$ and $(\tau_{bx}, \tau_{by}) = C_d\sqrt{u_b^2 + v_b^2}(u_b, v_b)$ are the x and y components of surface and bottom stresses. u_s and v_s the x and y components of the surface wind velocity, while u_b and v_b the x and y components of the bottom friction velocity. The

drag coefficient C_d is determined by matching a logarithmic bottom layer to the model at a height z_{ab} above the bottom, i.e.,

$$C_d = \max\left(k^2/\ln\left(\frac{z_{ab}}{z_o}\right)^2, 0.0025\right) \tag{2.17}$$

where z_o is the bottom roughness parameter, taken here as $z_o = 0.001$ m.

Freshwater was injected into the model domain from the coastal boundary as a volume flux defined as

$$U_o(t) = -\Delta y \int_{-H(x)}^{\eta} u dz \tag{2.18}$$

where Δy is the along-shelf grid resolution. The nutrient concentration of the freshwater N_f was specified at the mouth of the river.

A gravity wave radiation boundary condition plus a sponge layer were specified at the open boundary to allow waves to propagate out of the computational domain with minimum reflection (Chapman, 1985). A barotropic K_1 tidal elevation of 0.14 m was added at the open boundary to investigate effects of tidal mixing on spatial distribution of biological production.

d. Initial conditions

To simplify the model problem and focus on how the oceanic mixing affects the formation of the low-salinity front and associated biological production, we ignored the cross-shelf gradient of the background physical and biological variables. This simplification is consistent with our assumption that any horizontal variations in water masses and biological production should develop as a result of physical processes or physical and biological interactions.

Initial distributions of temperature and salinity were simply given by a vertically linear function with a temperature of 25.5°C and a salinity of 36.2 at the surface and 7.5°C and 34.9 at the bottom (500 m). The surface and bottom values of temperature and salinity used in the model were based on the observed hydrographic data taken at the 500-m isobath during the May 1993 interdisciplinary LATEX survey.

Initial distributions of biological state variables P, Z, and N, which were given by an analytical steady-state solution of the *P-Z-N* model (Franks *et al.,* 1986; Franks and Chen, 1996), are shown in Figure 4. The biological variables are considered based on their nutrient (N) components in μmole N l^{-1}. Since all biological variables were independent of temperature in the *P-Z-N* model and k_{ext} was constant across the shelf in our present modeling experiment, the initial P, Z, and N were horizontally uniform across the shelf.

e. Biological parameters

The choice of biological parameters is listed in Table 1. Because there was a wide range of values for some biological parameters, we first ran the model with an initial set of

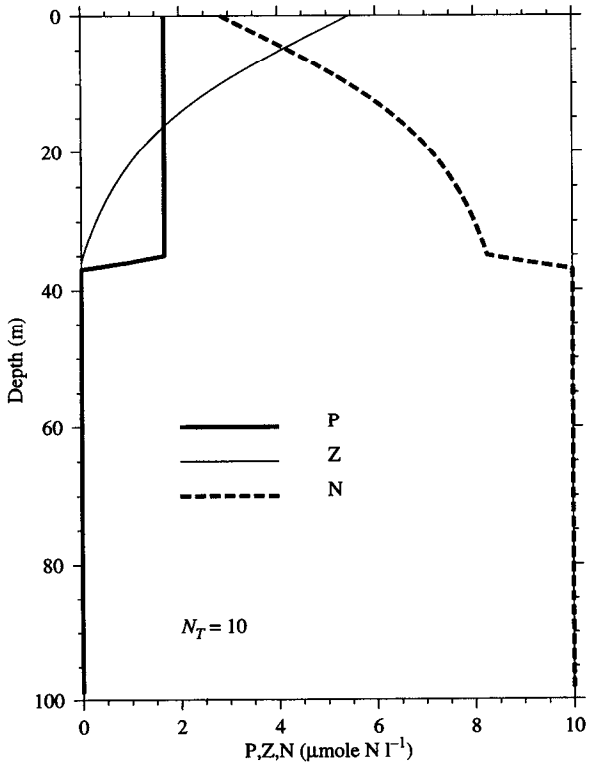

Figure 4. Initial conditions for the biological variables calculated by a steady state solution of the *P-Z-N* model. The total nutrient $N_T = 10$ μmole N l^{-1}.

parameters and then conducted some sensitivity analyses over ranges of parameters. Descriptions and discussions of our initial choices for the biological parameters are given here.

Based on profiles of observed nitrate concentrations on the outer LATEX shelf obtained from the May 1993 interdisciplinary survey, the total amount of nutrients was initially

Table 1. Parameters for the biological model.

Parameter	Description	Value
V_m	maximum phytoplankton growth rate	1.38 d^{-1}
k_s	half-saturation constant	1 μmole N l^{-1}
R_m	maximum grazing rate	0.5 d^{-1}
g	zooplankton death rate	0.2 d^{-1}
λ	Ivlev constant for grazing	0.5 (μmole N l^{-1})$^{-1}$
ϵ	phytoplankton death rate	0.1 d^{-1}
γ	unassimilated fraction by zooplankton	0.3
k_{ext}	diffuse attenuation coefficient	0.1 m^{-1}
N_T	initial total amount of nutrient	10 μmole N l^{-1}

given as $N_T = 10$ μmole N l^{-1}. The maximum phytoplankton growth rate V_m was chosen as 1.38 d^{-1} in our model. This value was estimated from recent observational data in the surface water at a shallower station (near the 20-m isobath) west of the Atchafalaya River (Brown, 1994). The diffuse attenuation coefficient $k_{ext} = 0.1$ m^{-1} was used for our model, which was calculated from the 1% light depths reported in Neuhard (1994) for spring.

Half saturation constant k_s for phytoplankton is a very species-specific parameter. Since over 300 species of phytoplankton were identified on the LATEX shelf (Bontempi, 1995), the estimation of this value from the literature is fairly general considering the number of species involved. According to Lalli and Parsons (1993), k_s ranges from 0.01 to 0.1 for oligotrophic waters and from 0.5 to 2.0 for eutrophic coastal water. The value of $k_s = 1.0$ was chosen for our model. This value represented a mean of oligotrophic middle-shelf water and eutrophic near-coastal water.

The maximum zooplankton grazing rate R_m and grazing efficiency of phytoplankton by zooplankton λ are variable parameters, which are reported to vary between 0.16 to 1.5 d^{-1} and 0.1 to 2 μmole N l^{-1}, respectively (McAllister, 1970; Frost, 1972; Checkley, 1980; Franks *et al.,* 1986). Fahnenstiel *et al.* (1992) described the mean zooplankton grazing rate for several different types of phytoplankton in the Gulf of Mexico. The zooplankton grazing rates on the dominant phytoplankton species were described further in Fahnenstiel *et al.* (1995). A mean grazing value of $R_m = 0.5$ d^{-1} and a grazing efficiency of $\lambda = 0.5$ were initially used in our model.

The assimilated fraction of phytoplankton by zooplankton $(1 - \gamma)$ is heavily influenced by the amounts of ingested phytoplankton and produced faeces. The efficiencies range from 30 to 80%, while the majority is between 60 and 70% (Raymont, 1980; Franks *et al.,* 1986). γ was chosen as 0.3 in our model, which represented an assimilated efficiency of 70%. This value was determined based on Franks *et al.* (1986) and Fuhrman (1992).

Phytoplankton and zooplankton death rates (ϵ and g) were derived from Franks *et al.* (1986). $\epsilon = 0.1$ d^{-1} was used for our model. This value gives an e-folding time scale of 10 days for phytoplankton. A wide range of values for g were used in previous modeling studies (Steele, 1974; Steele and Frost, 1977; Steele and Henderson, 1981; Franks *et al.,* 1986; Franks and Chen, 1996). The value of g used in those models ranged from 0.07 to 1.75 d^{-1}. Franks *et al.* (1986) chose $g = 0.2$ d^{-1} based on observational evidence of the zooplankton death rate under the condition of no food (Checkley, 1980; Dagg, 1977). The same value for g was used for our model, which represented an e-folding time scale of five days for zooplankton.

f. Design of numerical experiments

A schematic diagram of our coupled physical and biological model is shown in Figure 3. The model domain featured a section cut from north to south across the LATEX shelf near the Atchafalaya River. The bottom topography along the section was taken from the hydrographic survey data and smoothed for our modeling purposes. The water depth was 20 m at the coast, gradually increased to 200 m at the shelf break, and then rapidly dropped

to 500 m at the outer edge of the slope. Nonuniform grids were used in the cross-shelf direction. The cross-shelf resolution Δx was 2 km within the region from the coast to 60 km offshore, and then linearly increased to 20 km over an interval of 20 grid points outside the domain of interest. A uniform vertical grid was used. The vertical resolution $\Delta\sigma$ in the σ coordinate system was 0.0167 (61 points in the vertical), which corresponded to a vertical resolution of 8.3 m in the deep region at the 500-m isobath and 0.3 m near the coast at the 20-m isobath. The numerical experiments were conducted using a full 3-D model code with no along-shelf gradients. Three-grid points in the along-shelf direction were included in computation, and the along-shelf resolution Δy was 20 km.

The model was run as an initial value problem for a spring flooding case of the Atchafalaya River. The model was forced by a constant river discharge of 8,000 m^3/s at the coast. The outflow from the river contained a nitrate concentration of 20 μmole N l^{-1}. The water quality data, measured by the U.S. Geological Survey at Morgan City, LA at the head of the Atchafalaya Bay, showed that the nitrate concentration of freshwater discharge at the Atchafalaya River ranged from 77 to 100 μmole N l^{-1} during the period from April 28 to June 3, 1993. However, the nitrate concentration, measured at the northernmost station on Sec. 2 during the May 1993 LATEX interdisciplinary survey, was only about 14 μmole N l^{-1}. This difference suggests that the nitrate concentration of the riverine water decreased significantly when the water was carried out onto the inner shelf from the Atchafalaya Bay. Since the main focus in this study was on the interaction of physical and biological processes with a simple 2-D model approach, we have chosen the nitrate concentration for the freshwater flux based on the extrapolated value from two closed points at the northernmost stations on Sec. 2.

The river discharge of the Atchafalaya River in 1993 was about 14,000 m^3/s in April and May and declined to about 8,300 m^3/s in June. Observations showed that large amounts of freshwater were turned westward and flowed along the coast like a coastal trapped wave (Wiseman and Kelly, 1994; Wiseman and Garvine, 1995). Therefore, the actual offshore transport of freshwater on the 3-D shelf was much smaller than the flux measured in the river. Since a 2-D model was used, we chose a reduced river transport to best resolve the location of the low-salinity front within the onset time scale of the Atchafalaya riverine plume.

Both steady and variable winds were added into the model to examine effects of wind mixing and advection on the spatial distribution of biological production and phytoplankton biomass. Winds were imposed at the surface at the end of the 30th day when the density front was fully developed. A diurnal tidal forcing also was included later to estimate the contribution of tidal mixing to biological production.

3. Model results

a. Structure of the density front and currents

The model was first run prognostically as an initial value problem forced only by the constant river discharge. A density (low-salinity) front formed after 10 model days

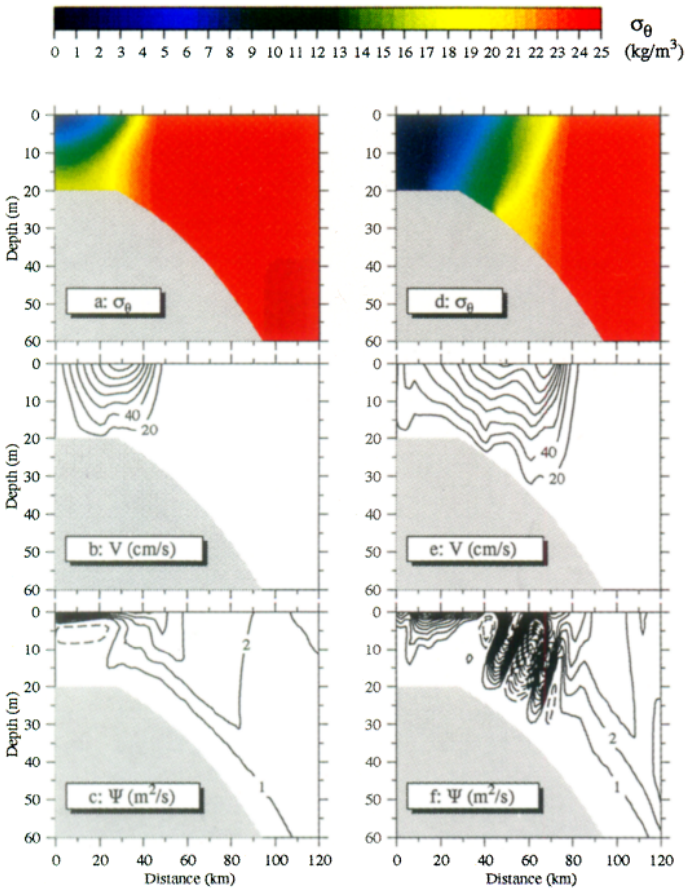

Figure 5. Distributions of the density (σ_θ: kg/m^3), the along-shelf current (v: cm/s), and the cross-shelf stream function (ψ: m^2/s) at the end of 10th (a–c) and 30th (d–f) model days.

(Fig. 5a). This front intensified and moved offshore with time as the total amount of freshwater on the inner shelf increased. A typical inner-shelf density field was fully developed at the 30th model day, with a strong, 30 km wide density frontal zone between the 20 to 50-m isobaths (Fig. 5d). Large cross-shelf density gradients within the frontal zone generated a strong along-shelf current, flowing westward with a maximum surface velocity of 160 cm/s at the 45-m isobath (Fig. 5e).

The cross-shelf current was characterized by a multiple-cell circulation pattern that developed with the evolution of the density front (Fig. 5c and f). When the density front formed on the 10th model day, the cross-shelf circulation consisted of two cells: a clockwise cell on the inshore side of the front and a counterclockwise cell on the offshore side of the front (when looking upstream). Multiple circulation cells were developed on the 25th day as a result of the increasing amount of freshwater on the shelf. Three significant cells were found within the frontal zone over a distance of about 50 km. This pattern remained unchanged as the density front moved slowly offshore with time (Fig. 5f).

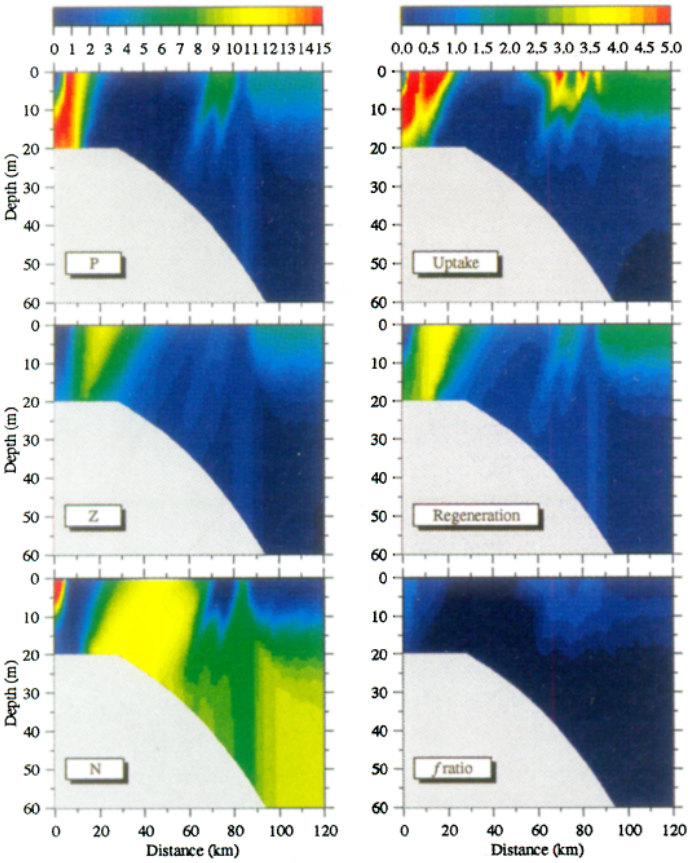

Figure 6. Distributions of the biological field at the end of the 30th model day. Left panels: top, phytoplankton (P); middle, zooplankton (Z); bottom, nutrients (N). Right panels: top, the nutrient uptake by phytoplankton; middle, the nutrient regeneration; bottom, the f ratio.

The cross-shelf circulation on the offshore side of the front was characterized by a weak counterclockwise current. This current flowed offshore at depth and returned to the onshore direction near the surface. On the inshore side of the front the model showed a clockwise current, which flowed onshore near the bottom and offshore near the surface. The maximum value of the cross-shelf current near the river was about 10 cm/s. The vertical velocity reached 0.02 cm/s within the frontal zone where multiple circulation cells were located.

b. Cross-shelf distributions of P, Z, and N

Figure 6 shows the color images of P, Z and N at the end of the 30th model day for the case forced only by the constant river discharge. All biological results are reported as μmole N l^{-1}. The biological field was significantly modified from its initial conditions. Close to the mouth of the river, maximum phytoplankton biomass concentrations (about 14

to 15 μmole N l^{-1}) developed throughout the whole water column. At the outer edge of the density front, a phytoplankton patch with a high biomass of 7 to 8 μmole N l^{-1} stretched downward from the surface to the depth of about 20 m. Phytoplankton biomass was lower within the frontal zone between 20 to 60-m isobaths. The mean biomass was only about 0.1 μmole N l^{-1}. Relatively high phytoplankton biomass also was found in the upper 15 m outside the frontal zone on the outer shelf.

Phytoplankton distributions were similar to the dissolved nutrient distributions. Lower nutrients were found throughout the whole water column in the inner-shelf region about 7 to 20 km offshore, in the upper 10 m at the outer edge of the density front, and on the outer shelf outside the frontal zone. The maximum nutrient levels were found in the upper 10 m over a region 7 km from the coast and were consistent with lower phytoplankton biomass in this area. A dome of high-nutrient water developed near the bottom within the frontal zone between 20- and 40-m isobaths. The maximum nutrient concentrations in the dome were about 12 μmole N l^{-1}. Distributions of the nutrients predicted by our model closely resembled those observed from the May 1993 LATEX interdisciplinary survey (see Fig. 1).

Distributions of the nutrients outside the frontal zone (about 90 km offshore) were characterized by a "tongue-like" structure. Dissolved nutrients, ranging from 6 to 11 μmole N l^{-1}, were advected upward from deep water and extended to the surface at the outer edge of the frontal zone (Fig. 6, *N* at 90 km). This upwelling resulted in a large gradient of the nutrients at the edge of the density front between low-salinity inner-shelf and high-salinity outer-shelf waters.

Zooplankton biomass reached a maximum of about 8 to 10 μmole N l^{-1} in the region between 10 and 30 km from the coast. A patch with a moderately high biomass of 3 to 4 μmole N l^{-1} also was found at the outer edge of the density front. This zooplantkon patch corresponded to the high biomass of phytoplankton in that region. It should be pointed out here that no swimming or other zooplankton behavior was included in the present model. Since no zooplankton data were available from the May 1993 LATEX interdisciplinary survey, it was difficult to check our model for zooplankton prediction. For this reason, we will focus our discussion here on nutrients and phytoplankton.

c. Nutrient uptake and regeneration

Nutrient uptake by phytoplankton is defined by the first term on the right-side of the phytoplankton equation (2.10). In the Franks and Chen (1996) model, nutrient uptake is equal to the nitrate uptake controlled by the maximum phytoplankton growth rate, the incident irradiance, the half-saturation constant, the phytoplankton biomass, and the nitrate concentration. The regeneration of nutrients is defined as the sum of zooplankton excretion and death of phytoplankton and zooplankton on the right-side of the nutrient equation (2.12). Franks and Chen (1996) also calculated the *f*-ratio: the ratio of new production to total production. Total production in their model was defined as the nitrate uptake by phytoplankton, and new production equaled the difference between total production and regenerated nutrients. We adopted their definition in the present study.

The right panel of Figure 6 shows the nutrient uptake rate and regeneration as well as the *f*-ratio estimated on a basis of the values of *P*, *Z*, and *N* at the end of the 30th day. The highest nutrient uptake (about 5 μmole N l^{-1} d^{-1}) was found throughout the whole water column within a relatively wide region near the coast, and also in the upper 10 m at the outer edge of the density front. Between these two high nutrient uptake zones was a wider region characterized by a very low uptake rate. The mean value of nutrient uptake in that region was about 0.5 μmole N l^{-1} d^{-1} near the surface but decreased to 0.01 μmole N l^{-1} d^{-1} near the bottom.

Cross-shelf distributions of nutrient regeneration were similar to those of nutrient uptake and zooplankton biomass. The highest regeneration rate of 4 μmole N l^{-1} d^{-1} was found throughout the water column in a region between 10 and 30 km away from the coast. A patch of water with a relatively high regeneration rate, which ranged from 1 to 2.5 μmole N l^{-1} d^{-1} also was found in the upper 15 m at the outer edge of the density front. A dome-like region characterized by very low regeneration rates was observed between the inner and outer shelves. The value of nutrient regeneration in this area was about 0.01 μmole N l^{-1} d^{-1} near the bottom and increased to 0.5 μmole N l^{-1} d^{-1} near the surface.

Using the Franks and Chen (1996) definition described above, we also calculated the *f*-ratio across the shelf. The results also showed two regions with high rates of new production: one near the coast and another at the outer edge of the density front. The first was wider at the surface and became narrower with depth. The offshore zone was limited to the upper 15 m. It was widest at the surface and extended downward like a tongue. The *f*-ratio in these two regions was about 0.7 to 0.9. Between these two high production zones was a wider region with a very low level of new production. This region occupied a large portion of the frontal zone, suggesting that the bottom-rich nutrient pattern found within the frontal zone was caused by the interaction of physical and biological processes rather than biological production alone.

d. Comparisons with observations

A data set for nitrate and chlorophyll *a* was taken from bottle samples during the May 1993 interdisciplinary survey on the LATEX shelf. The horizontal resolution of these samples was about 5 to 10 km in nitrate and about 20 to 30 km in chlorophyll *a*. The data taken on Sec. 2, the closest section to the Atchafalaya River, were used for comparison with our model results. The distribution of observed nitrate near the bottom agreed both qualitatively and quantitatively with model results in the inner shelf within the frontal zone (Fig. 7a). The distribution of observed chlorophyll *a* near the surface also agreed well with model results in the inner shelf within the frontal zone (Fig. 7b). While the qualitative predicted and observed patterns of nutrients were the same on the outer shelf, the predicted concentration of nutrients was higher than that observed in the LATEX shelf study. Similarly, the predicted phytoplankton biomass on the outer shelf was too high when compared to the observed chlorophyll *a* data.

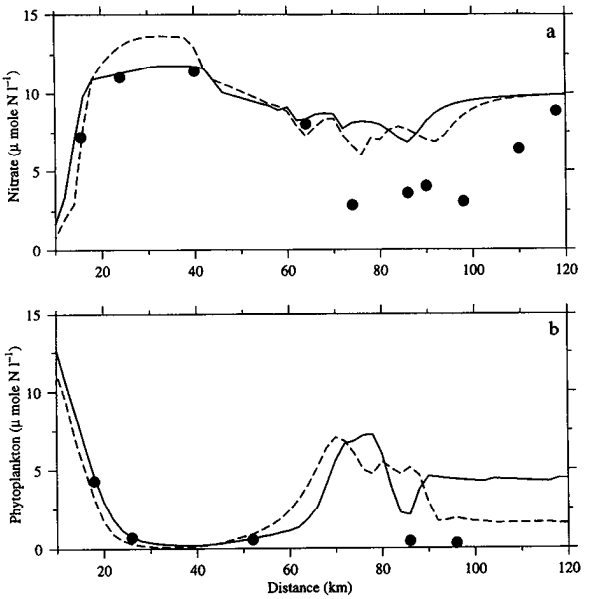

Figure 7. Comparison between model results and observations for (a) the nitrate at the bottom; and (b) the averaged phytoplankton in the upper 10 m. The model-predicted data are represented by solid (nonsinking) and dashed (sinking) lines. The observed data are indicated by filled circles and were taken from bottle samples on Sec. 2, the May 1993 interdisciplinary LATEX survey.

Poor agreement between observed data and the model's predictions in phytoplankton can be accounted for by insufficient sampling and the fact that the sinking behavior of phytoplankton was not taken into account. Since the chlorophyll *a* samples were taken with a separation scale of about 30 km between 35- and 55-m isobaths, the observation failed to resolve the high biomass patch of phytoplankton at the outer edge of the density front.

To examine the effect of sinking on the predicted patterns, a sinking speed of 1 m d^{-1} was included for phytoplankton on the 30th model day. The inclusion of such a constant sinking velocity resulted in a subsurface phytoplankton maximum outside the density frontal zone. This addition provided much better agreement between model results and observations (Fig. 7). In addition, sinking showed very little influence on the distribution of phytoplankton in the inner shelf. This suggests that sinking was not a prerequisite for the formation of a high phytoplankton zone near the river or for the patch at the outer edge of the density front. The increase of nutrient concentrations near the bottom between 20 to 40-m isobaths at the end of the 35th day, which was an expression of the phytoplankton's tendency to sink, resulted from the evolution of nutrients over time and was not related to the sinking of phytoplankton.

e. Wind effects

The synoptic-scale meteorological field on the LATEX shelf in spring and summer was dominated by a southeasterly wind. Such a wind field, however, was intermittently altered

by atmospheric frontal passages associated with low-pressure cells (Chen *et al.*, 1996). The typical time scale of a frontal passage was about 5 to 7 days. In general, the wind was southeastward during the first 2 to 3 days and then reversed to become northwestward after the front passed. Although some efforts have been made to relate oceanic responses of the LATEX shelf to local and global winds (Cochrane and Kelly, 1986; Chen *et al.*, 1996; Lewis and Reid, 1985), effects of the wind on biological processes have not been well explored on the LATEX shelf.

To examine the contribution of the wind to the LATEX shelf biological processes, we added surface wind stress to the model at the end of the 30th day, at a time when the density front was fully developed and the bottom-rich nutrient pattern had formed within the frontal zone. Three types of wind forcing were considered: (1) upwelling-favorable winds, (2) downwelling-favorable winds, and (3) variable winds associated with frontal passages. The wind direction was defined by the degree from which the wind blew and was measured clockwise from the north. The upwelling-favorable wind referred to the wind blowing eastward along the shelf, while the downwelling-favorable wind referred to the wind blowing westward. The magnitude of the wind was specified as 5 m/s for all three cases.

i. Upwelling-favorable winds. When a constant, upwelling-favorable wind started blowing at the surface, the density and current fields were significantly altered. The buoyancy-induced, along-shelf westward current dramatically weakened over the shelf, especially near the coast where the current turned to the east in the same direction as the wind. The density front was pushed away from the coast by the offshore, near-surface Ekman transport, and the deep denser water flowed onto the shelf in the subsurface along the bottom (Fig. 8a). This process resulted in a single circulation cell across the shelf, with a relatively strong upwelling near the coast, a narrow offshore flow at the surface, and a compensatory onshore flow in the deep region.

The biological field also was altered in response to the changes in the physical field. The wind tended to speed up the offshore migration of phytoplankton and nutrients in the upper layer and the onshore advection in the lower layer from the mid-depth to the bottom. This process significantly reduced the horizontal gradient and increased the vertical gradient of both phytoplankton and nutrients. As a result, a long lens of high phytoplankton biomass formed in the upper 10 m within the low-salinity water (Fig. 8b). The dome-like bottom-rich nutrient pattern, which was originally located on the 20 to 40-m isobaths, was stretched shoreward to the coast due to the wind-induced upwelling (Fig. 8c).

ii. Downwelling-favorable winds. In this case, the wind advected dense oceanic water onshore in the upper layer and enhanced vertical mixing in the frontal zone. As a result, the density contours became straight, near-vertical lines intersecting with the surface and the bottom over much of the shelf (Fig. 8d).

Wind-enhanced turbulent mixing also produced a vertically uniform structure of phytoplankton and nutrients over the shelf (Fig. 8e and 8f). The region of high phytoplank-

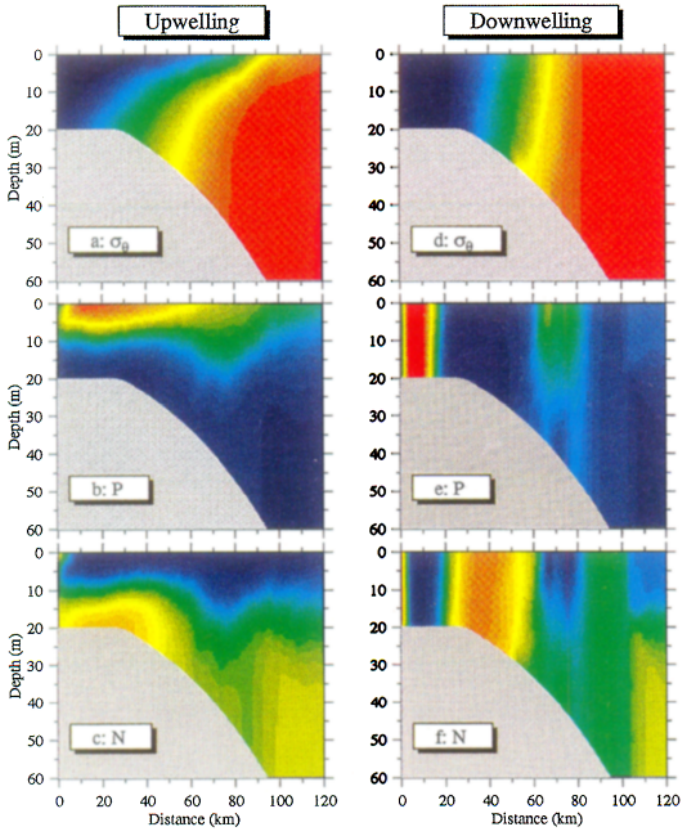

Figure 8. Distributions of density (σ_θ: kg/m^3), phytoplankton (P: μmole N l^{-1}), and nutrients (N: μmole N l^{-1}) at the end of the 35th model day for upwelling (left panels) and downwelling (right panels) cases. The wind was imposed into the model at the end of the 30th day. The scales of the color image are the same as those in Figure 5 (for σ_θ) and Figure 6 (for P and N).

ton biomass near the coast, which was originally narrower near the surface and wider near the bottom, became much more uniform in both vertical and horizontal directions. A patch of high phytoplankton biomass formed at the outer edge of the density front and extended downward to a depth of 40 m. The bottom-rich nutrients between the 20- and 40-m isobaths were well mixed to the surface and led to a vertically-uniform nutrient distribution within the frontal zone.

iii. Variable winds. The variable wind used in this study was specified as a sinusoid function with a period of 5 days. The wind started blowing eastward at the end of the 30th day and reversed to become westward midway into the 32nd day. The maximum eastward wind (upwelling-favorable) occurred at 31.25 days, 30 hours after the wind started, while

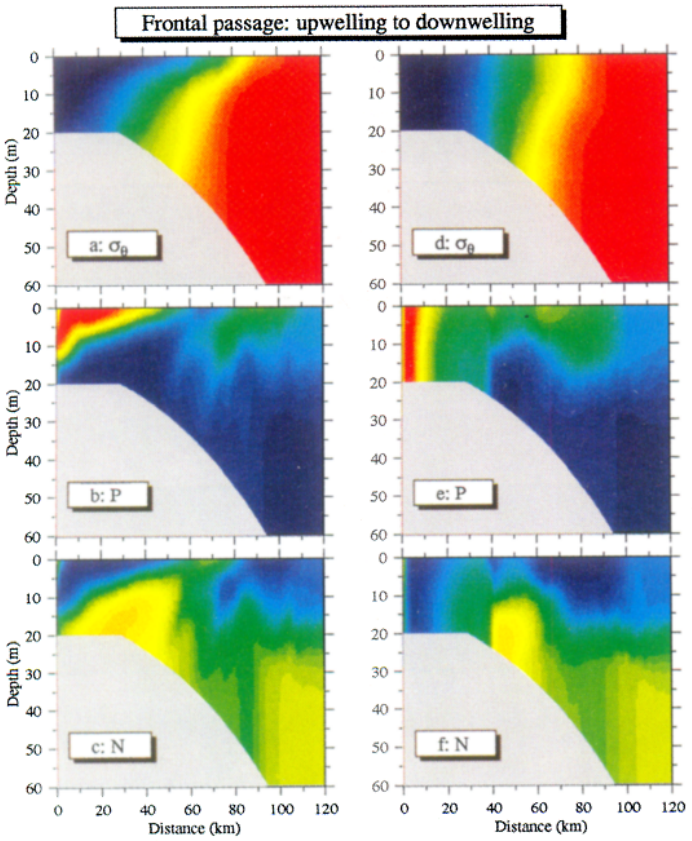

Figure 9. Distributions of density (σ_θ: kg/m^3), phytoplankton (P: μmole N l^{-1}), and nutrients (N: μmole N l^{-1}) for the variable wind case. Left panels: at the time of the maximum upwelling-favorable wind. Right panels: at the time of the maximum downwelling-favorable wind. The variable wind used in this study was specified as a sinusoid function with a period of 5 days. The scales of the color image are the same as Figure 8.

the westward wind (downwelling-favorable) reached its maximum at 33.75 days, 90 hours after the wind started blowing.

The varying wind stress during the period of upwelling tended to speed up the offshore movement of low-salinity water in the upper layer and the onshore movement of dense water in the deep region. This process resulted in a density front that was "tilted" toward the offshore direction (Fig. 9a). A broad, high-biomass patch of phytoplankton, which was wider near the surface and became narrower with depth, was found near the coast (Fig. 9b). The bottom-rich nutrient pattern was compressed in the vertical and stretched shoreward in the horizontal (Fig. 9c).

When the wind reversed to become westward, both the physical and biological fields responded rapidly. Density, phytoplankton, and nutrients became vertically uniform near

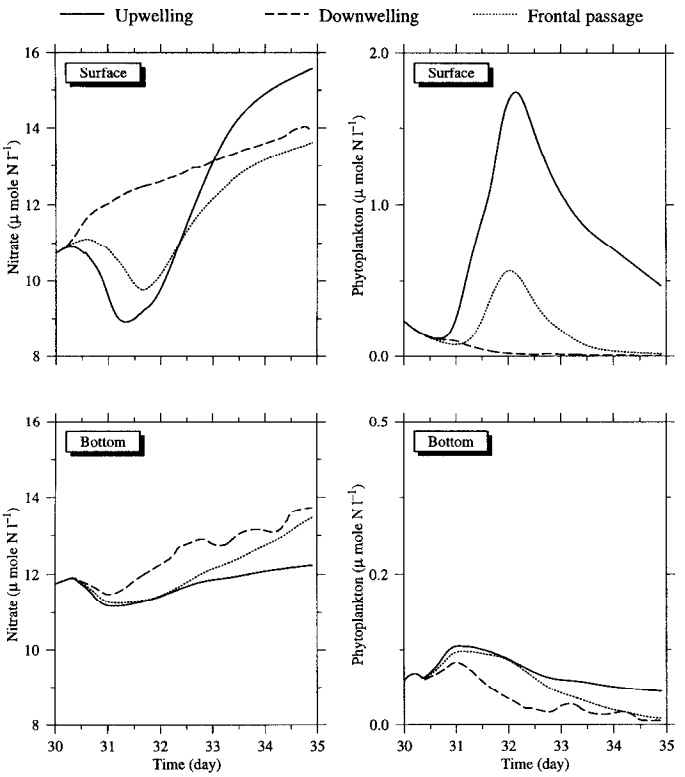

Figure 10. Time sequences of nutrients and phytoplankton at a location about 5 km away from the coast for the upwelling (solid line), downwelling (dashed line), and variable wind (dotted line) cases. Upper panels: at surface. Lower panels: at bottom.

the coast just one day after the wind reversed (Fig. 9d, e, f). However, since the duration of downwelling wind was too short to mix biological variables in the region deeper than 20 m, the bottom-rich nutrient pattern still existed within the frontal zone, although its size was reduced significantly (Fig. 9f).

The evolution of the biological field under different wind forcings also was examined. For example, time sequences of N and P at the surface and bottom at a location 5 km offshore are shown in Figure 10 for upwelling, downwelling, and variable winds. In the upwelling case, nutrients at the surface decreased to 9 μmole N l^{-1} in the first 1.5 days and then rapidly increased to 15.5 μmole N l^{-1}. Correspondingly, phytoplankton at the surface rapidly increased to 1.7 μmole N l^{-1} in the first two days and then decreased. Time series of nutrients and phytoplankton at the bottom were very similar to those at the surface, except for smaller amplitudes and phase shifts.

Enhanced vertical mixing due to downwelling winds caused an increase in nutrients but a decrease in phytoplankton during the entire time, even though the phytoplankton growth rate was much smaller in the downwelling case than in the upwelling case. Nutrient levels

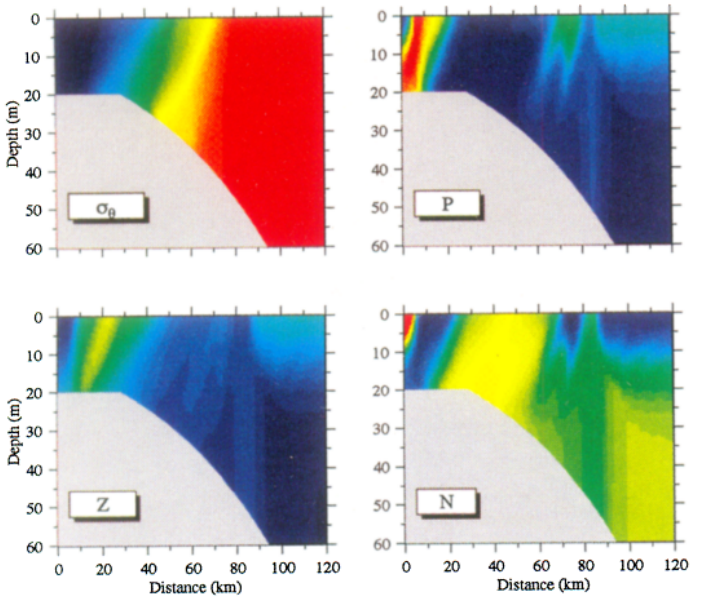

Figure 11. Distributions of density (σ_θ: kg/m^3), phytoplankton (P: μmole N l^{-1}), zooplankton (Z: μmole N l^{-1}), and nutrients (N: μmole N l^{-1}) at the end of the 35th model day for the case with both river discharge and diurnal tidal forcings. The scales of the color image are the same as Figure 8.

were as high as 14 μmole N l^{-1} at the end of the 35th day, while the phytoplankton biomass dropped to almost zero after 5 days. The variation of phytoplankton and nutrients in the variable wind case was very similar to those values in the upwelling and downwelling cases, even though the duration of upwelling and downwelling winds in this case was shorter.

f. Tidal effects

Tides are weak on the LATEX shelf (Reid and Whitaker, 1981). Previous observations of sea surface elevation near the coast showed that the most significant tidal constituents in this region were diurnal tides. Reid and Whitaker (1981) numerically simulated the astronomical tides in the Gulf of Mexico. By tuning their model to best fit the available coastal tidal data, they provided cotidal charts of semidiurnal and diurnal tides for the entire Gulf. The cotidal charts for diurnal O_1 and K_1 showed that, at the central LATEX shelf, the amplitude of the tidal elevation was about 14 cm at the 500-m isobath and then increased to 18 cm at the coast. Based on this information, we added tidal forcing into our model by specifying a barotropic K_1 tidal elevation with an amplitude of 14 cm at the southern open boundary.

The inclusion of diurnal tidal forcing in our model made little change of the distribution of the biological fields (Fig. 11). The weak tidal mixing did reduce the nutrient concentra-

tion in the dome near the bottom. Phytoplankton distributions were slightly enhanced near the coast, and the region of maximum zooplankton biomass shrank horizontally near the surface.

4. Sensitivity analyses

Qualitatively, our model results exhibit a high level of correlation with observations for nutrients and phytoplankton on the onshore side of the density front. Basic distribution patterns of N and P remained similar within and outside the frontal zone under a wide range of biological parameters, even though the biomass values were more sensitive to model parameter changes. To test the model sensitivity to uncertainties in our biological variables, we have run the model using ranges of the maximum growth rate of phytoplankton V_m, the maximum grazing rate R_m, the grazing efficiency of phytoplankton by zooplankton λ, the half-saturation constant of phytoplankton k_s, the efficiency of ingestion $(1 - \gamma)$, and the nutrient concentration of freshwater discharge N_f. Some of these results are shown in Figure 12.

Previous studies in the Gulf of Mexico suggested that the maximum phytoplankton growth rate ranged from about 0.1 to 3.0 d^{-1} (Fahnenstiel *et al.*, 1992, 1995; Brown, 1994; Bierman *et al.*, 1994). Bierman *et al.* (1994) applied a preliminary mass balance model to study primary productivity and dissolved oxygen in the Mississippi River plume over the inner LATEX shelf. They found that maximum growth rates at ambient temperatures can be up to 3.0 d^{-1} due to high water temperatures during summer. These growth rates were significantly reduced by nutrient and light limitations. The actual specific growth rates ranged between 1.0 d^{-1} and 1.2 d^{-1} in the inner shelf near the Mississippi Delta. These values are close to the observed value (1.38 d^{-1}) found by Brown (1994) at a measurement station west of the Atchafalaya River. Based on these data, we suggest that maximum phytoplankton growth rates over the inner LATEX shelf range between 1.0 d^{-1} and 1.4 d^{-1}.

Setting the maximum phytoplankton growth rate, V_m, to 1.0 d^{-1} resulted in no changes in the basic patterns of the biological field within and outside the density frontal zone at the end of the 30th model day, compared to the case with $V_m = 1.38\ d^{-1}$. However, the variation of P and N over time was significantly modified. The time at which the maximum nutrient and phytoplankton levels occurred was delayed about 5 days compared with the case of $V_m = 1.38\ d^{-1}$. Because of that, the intensity of the dome-like N pattern near the bottom on the shelf and the high biomass P peak near the surface at the front at the 30th day were lower than those for the case of $V_m = 1.38\ d^{-1}$.

We also used this model to test for the grazing efficiency of phytoplankton by zooplankton (λ). Previous studies suggested a range of λ between 0.1 and 2 $(\mu mole\ N\ l^{-1})^{-1}$ in the inner LATEX shelf (Fahnenstiel *et al.*, 1995). Increasing λ from 0.5 to 0.8 has little effect on the cross-self patterns of phytoplankton, zooplankton and nutrients near the coast and inside the frontal zone. Similar to the case with a reduced V_m, increasing λ tended to slow down the growth of phytoplankton near the front.

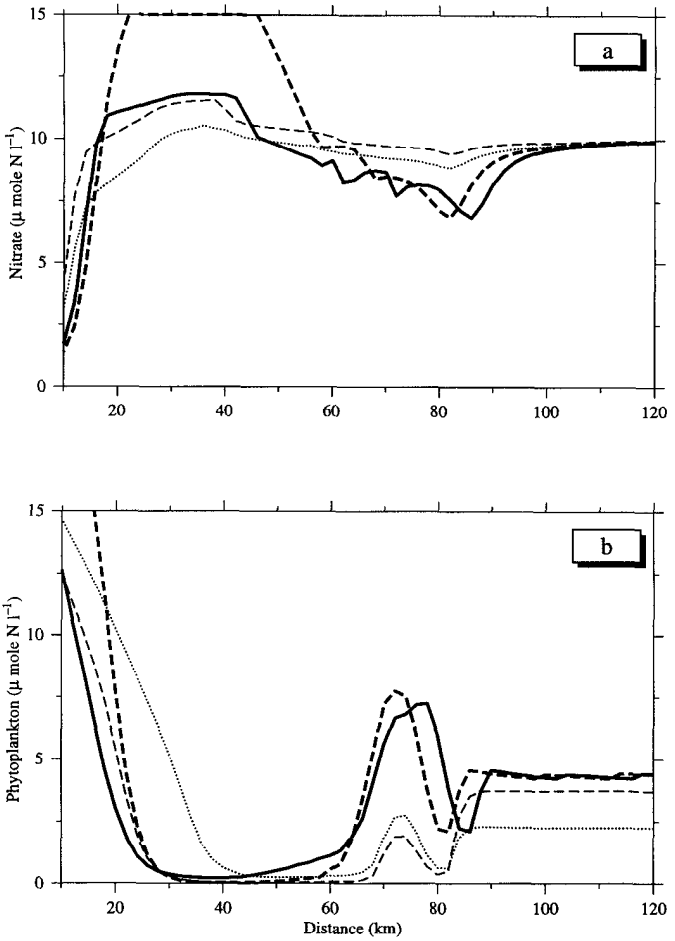

Figure 12. Cross-shelf distributions of the near-bottom nitrate (a) and the average phytoplankton in the upper 10 m (b) at the end of the 30th model day. Heavy solid line represents the case with V_m = 1.38 d^{-1}, R_m = 0.5 d^{-1}, λ = 0.5 (μmole N l^{-1})$^{-1}$, and N_f = 20 μmole N l^{-1}. Dotted, dashed, and heavy dashed lines represent the cases with modified values of V_m = 1.0 d^{-1}, λ = 0.8 (μmole N l^{-1})$^{-1}$, and N_f = 40 μmole N l^{-1}, respectively. Note that (a) and (b) were truncated at the level of 15 μmole N l^{-1}.

Basic patterns of the biological fields were also insensitive to an increased nitrate concentration of freshwater discharges. When N_f was increased from 20 μmole N l^{-1} to 40 μmole N l^{-1}, the basic patterns of P, Z, and N remained unchanged, even though the P, Z, and Z levels increased significantly. We also ran the model with even higher values of N_f (for example, N_f = 60 μmole N l^{-1}) and found that the resulting patterns of P, Z, and N were just like the same, but higher values than those model runs with smaller N_f concentrations. The fact that the cross-shelf distribution of P, Z, and N was insensitive to changes in biological parameters suggests that the model results are robust.

5. Discussion

Similar to the LATEX shelf observations, our coupled biological-physical model predicted a dome-like pattern of nitrate with a maximum concentration near the bottom within the frontal zone. The fact that this dome was located in the region with a very low new production rate of nutrients suggests that the occurrence of such a pattern was closely related to the interaction of biological and physical processes.

Cross-shelf circulation as predicted by the model was characterized by a surface-intensified offshore current near the coast and multiple cells inside the frontal zone (Fig. 5f). Cross-shelf currents were very weak near the bottom, even in the frontal zone where multiple cells existed. In addition to recycled and new production of nutrients through biological processes, the model shows that nutrients in the frontal zone were supported physically by two sources: (1) horizontal advection from the river discharge, and (2) advection- and diffusion-induced upward nutrient flux outside the frontal zone on the shelf. Multiple cells in the frontal zone acted like a retention zone that recirculated the nutrients in the vertical and also restricted marine organisms from cross-frontal exchanges. However, since these cells were not completely closed in the vertical, especially near the bottom and surface, a portion of the marine organisms might settle near the bottom in the weak flow region as they were advected along instantaneous streamlines from the river into the frontal zone.

The *e*-folding vertical scale of light efficiency was about 10 m in our model. This light limitation restricted the efficient utilization of nutrients by phytoplankton to the upper 10 m of the euphotic zone. Since the uptake rate of nutrients by phytoplankton was larger near the surface than near the bottom, nutrients were rapidly utilized by phytoplankton when they were advected to the upper layer either from the outside sources or via recirculation by multiple cells. Consequently, there was no possibility for a high nutrient concentration dome to form near the surface in the frontal zone where cross-shelf currents were dominated by multiple cells.

It took a relatively long period of about 25 to 30 days to form a high concentration dome of nutrients in the weak flow region near the bottom inside the frontal zone. This lag suggests a coupled biological and physical driving mechanism associated with the cross-shelf secondary circulation in the frontal zone and the spatial variation of nutrient uptake and regeneration. Physical processes caused the formation of a large concentration of nutrients in the weak current region within the frontal zone. Subsequent biological processes limited the increase of nutrients in the upper euphotic zone and hence led to the bottom-rich nutrient pattern.

It should be remembered that our present model ignored the along-shelf advection of nutrients from the Mississippi River and potential fluxes of nutrients from the bottom sediments. In spite of this, our 2-D model successfully reproduced the basic observed patterns of nutrients and phytoplankton in the inner LATEX shelf where the Atchafalaya River discharge was dominant. This success suggests that the 2-D model has captured the basic dynamics of biological and physical processes in that particular region.

6. Summary

A simple 2-D coupled physical and biological model has been used to assess the main features of phytoplankton and nutrient distributions over the inner LATEX, where the river discharge was a dominant physical process. The model reproduced a well-defined dome of high nutrient concentration near the bottom within the frontal zone. The model also predicted a high biomass patch of phytoplankton that developed near the surface at the outer edge of a density front on the LATEX shelf.

The model results were in reasonable agreement with field measurements taken from the May 1993 interdisciplinary survey on the LATEX shelf. The formation of bottom-rich nutrient pattern in the frontal zone was probably caused by the interaction of physical and biological processes. Physical processes caused the formation of a large concentration of nutrients in the weak current region within the frontal zone. Subsequent biological processes limited the increase of nutrients in the upper euphotic zone and hence led to the bottom-rich nutrient pattern.

The coupled model showed that both nutrient uptake and regeneration were higher throughout the water column near the coast and in the upper layer at the outer edge of the density front. The maximum nutrient uptake value was about 5 μmole N l^{-1} d^{-1}. The maximum nutrient regeneration was about 3.5 to 4.0 μmole N l^{-1} d^{-1} near the coast and 1.5 to 2 μmole N l^{-1} d^{-1} at the outer edge of the density front. New production was high near the coast and in the upper 10 m at the outer edge of the density front. Most of the region inside the frontal zone, especially near the bottom, was characterized by low nutrient uptake and regeneration as well as low new production.

Cross-shelf distributions of the biological field were significantly modified by upwelling-favorable wind, due to Ekman transport. The downwelling-favorable wind tended to enhance the vertical mixing and caused a more vertically uniform pattern of nutrients, phytoplankton, and zooplankton. Modification of the biological field due to variable winds associated with atmospheric frontal passages depended on the amplitude and duration of winds. The model revealed that tidal mixing is too weak to make a significant contribution to the basic distribution of biological production within the frontal zone over the inner LATEX shelf.

Acknowledgments. This research was supported by the Office of Naval Research (ONR) under grant number N00014-93-1-0513 and subcontract number RR50905F to University of Georgia (C. Chen) and subcontract number I400257 to University of Southern Mississippi (D. Wiesenburg) from The Texas A&M Research Foundation. C. Chen would like to thank Dr. Peter Franks for sharing his knowledge on oceanic biological processes and also for his encouragement and support during this study. Chen also would like to thank Drs. R. Beardsley and K. Wishner, who initially galvanized his interest in biological and physical interactions, and Dr. W. J. Wiseman, who carefully read through this manuscript and provided many valuable comments and suggestions. We thank Paula S. Bontempi who compiled most of the biological data used in the model. Comments and suggestions from Drs. D. Bronk and B. Binder are greatly appreciated. We also want to thank two anonymous reviewers for their valuable comments, and Mr. George Davidson and Dr. W. J. Wiseman for their editorial help on this manuscript. Physical and biological data used in this study were collected

during the Louisiana-Texas Shelf Circulation and Transport Process Study (LATEX A) at Texas A&M University. The LATEX A program was supported by the Minerals Management Service of the U.S. Department of the Interior, under OCS contract number 14-35-0001-30509.

REFERENCES

Bierman, V. J. Jr., N. N. Rabalais, S. C. Hinz, R. E. Turner and W. J. Wiseman, Jr. 1994. A preliminary mass balance model of primary productivity and dissolved oxygen in the Mississippi River plume/inner gulf shelf region. Estuaries, *17,* 886–899.

Blumberg, A. F. 1994. A primer for ECOM-si. Technical Report of HydroQual, Inc., 66 pp.

Blumberg, A. F. and G. L. Mellor. 1987. A description of a three-dimensional coastal ocean circulation model, *in* Three-Dimensional Coastal Ocean Model, N. S. Heaps, ed., Coast. Estuar. Sci., *4,* 1–16.

Bontempi, P. S. 1995. Phytoplankton distributions and species composition across the Texas-Louisiana continental shelf during the floor regimes of the Mississippi River. M.S. thesis, Texas A&M University, 261 pp.

Brown, S. L. 1994. Microzoplankton grazing along the northwestern continental shelf of the Gulf of Mexico. M.S. thesis, University of Texas at Austin, 124 pp.

Casulli, V. 1990. Semi-implicit finite-difference methods for the two-dimensional shallow water equations. J. Comp. Phys., *86,* 56–74.

Chapman, D. C. 1985. Numerical treatment of cross-shelf open boundaries in a barotropic coastal model. J. Phys. Oceanogr., *15,* 1060–1075.

Checkley, D. M. 1980. The egg production of a marine planktonic copepod in relation to its food supply: laboratory studies. Limnol. Oceanogr., *25,* 430–446.

Chen, C. and R. Beardsley. 1995. Numerical study of stratified tidal rectification over finite-amplitude banks. Part I: Symmetric banks. J. Phys. Oceanogr., *25,* 2090–2110.

Chen, C., R. Beardsley and R. Limeburner. 1995. Numerical study of stratified tidal rectification over finite-amplitude banks. Part II: Georges Bank. J. Phys. Oceanogr., *25,* 2111–2128.

Chen, C., R. Reid and W. D. Worth, Jr. 1996. Near-inertial oscillations over the Texas-Louisiana shelf. J. Geophys. Res., *101,* 3509–3524.

Cochrane, J. D. and F. J. Kelly. 1986. Low-frequency circulation on the Louisiana-Texas shelf. J. Geophys. Res., *88,* 2615–2620.

Dagg, M. 1977. Some effects of patchy food environments on copepods. Limnol. Oceanogr., *22,* 99–107.

Dinnel, S. P. and W. J. Wiseman, Jr. 1986. Fresh water on the Louisiana and Texas shelf. Cont. Shelf Res., *6,* 765–784.

Fahnenstiel, G. L., M. H. Marcowitz, M. J. McCormick, D. G. Redalje, S. E. Lohrenz, H. J. Carrick and M. J. Dagg. 1992. High growth and microzoplankton grazing loss rate for phytoplankton populations from the Mississippi River plume region, *in* Nutrient Ehanced Coastal Ocean Productivity Publication Number TAMU-SG-91-109. Sea Grant Program TAMU Calveston, Texas, 111–116.

Fahnenstiel, G. L., M. J. McCormick, G. A. Lang, D. G. Redalje, S. E. Lohrenz, M. H. Marcowitz, B. Wagoner and H. J. Carrick. 1995. Taxon-specific growth and loss rates for dominant phytoplankton populations from the northern Gulf of Mexico. Mar. Ecol. Prog. Ser., *117,* 229–239.

Flint, R. W. and D. Kamykowski. 1984. Benthic nutrient regeneration in south Texas coastal waters. Estuar. Coast. Shelf Sci., *18,* 221–230.

Franks, P. J. S. and C. Chen. 1996. Plankton production in tidal fronts: A model of Georges Bank in summer. J. Mar. Res., *54,* 631–651.

Franks, P. J. S., J. S. Wroblewski and G. R. Flierl. 1986. Behavior of a simple plankton model with food-level acclimation by herbivores. Mar. Biol., *91,* 121–129.

Frost, B. W. 1972. Effects of size and concentration of food particles on the feeding behavior of the marine planktonic copepod *Calanus pacificus.* Limnol. Oceanogr., *17,* 805–815.

Fuhrman, J. 1992. Bacterioplankton roles in cycling of organic matter: the microbial food web, *in* Primary Productivity and Biogeochemical Cycle in the Sea, P. G. Falkowski and A. D. Woodhead, eds., Plenum Press, New York, 361–384.

Galperin, B., L. H. Kantha, S. Hassid and A. Rosati. 1988. A quasi-equilibrium turbulent energy model for geophysical flows. J. Atm. Sci., *45,* 55–62.

Kamykowsji, D. and J. L. Bird. 1981. Phytoplankton associations with the variable nepheloid layer on the Texas continental shelf. Estuar., Coast. Shelf Sci., *13,* 317–326.

Lalli, C. M. and T. R. Parsons. 1993. The effects of nutrients on growth rates, *in* Biological Oceanography—An Introduction, Pergamon Press, New York, p. 63.

Lewis, J. K. and R. O. Reid. 1985. Local wind forcing of a coastal sea at subinertial frequencies. J. Geophys. Res., *94,* 8163–8178.

Lohrenz, S. E., M. J. Dagg and T. E. Whitledge. 1990. Enhanced primary production at the plume/oceanic interface of the Mississippi River. Cont. Shelf Res., *10,* 639–664.

McAllister, C. D. 1970. Zooplankton rations, phytoplankton mortality and the estimation of marine production, *in* Marine Food Chains, J. H. Steele, ed., Berkley: University of California Press.

Mellor, G. L. and T. Yamada. 1974. A hierarchy of turbulence closure models for planetary boundary layers. J. Atm. Sci., *33,* 1791–1896.

—— 1982. Development of a turbulence closure models for geophysical fluid problem. Rev. Geophys. Space Phys., *20,* 851–875.

Neuhard, C. A. 1994. Phytoplankton distributions across the Texas-Louisiana shelf in relation to coastal physical processes. MS thesis, Texas A&M University, 205 pp.

Raymont, J. E. G., ed. 1980. Plankton and Productivity in the Oceans: Vol. 2: Zooplankton, Pergamon Press, New York.

Reid, R. O. and R. E. Whitaker. 1981. Numerical model for astronomical tides in the Gulf of Mexico: theory and application. Technical report of the department of oceanography, Texas A&M University, College Station, TX 77843, 115 pp.

Riley, G. A. 1937. The significance of the Mississippi River drainage for biological conditions in the northern Gulf of Mexico. J. Mar. Res., *1,* 60–74.

Rowe, G. T., C. H. Clifford and K. L. Smith Jr. 1975. Benthic nutrient regeneration and its coupling to productivity in coastal waters. Nature, *225,* 215–217.

Sahl, L. E., W. J. Merrell and D. C. Biggs. 1993. The influence of advection on the spatial variality of nutrient concentrations on the Texas-Louisiana continental shelf. Cont. Shelf Res., *13,* 233–251.

Shiderler, G. L. 1975. Development of the benthic nepheloid layer on the south Texas continental shelf, western Gulf of Mexico. Mar. Geol., *41,* 37–61.

Sklar, F. H. and R. E. Turner. 1981. Characteristics of phytoplankton off Barataria Bay in an area influenced by the Mississippi River. Contr. Mar. Sci., *24,* 93–106.

Steele, J. H. 1974. The Structure of Marine Ecosystems, Cambridge, Harvard University Press, 128 pp.

Steele, J. H. and B. W. Frost. 1977. The structure of plankton communities. Phil. Trans. R. Soc. Lond., *280,* 485–534.

Steele, J. H. and E. W. Henderson. 1981. A simple plankton model. Am. Nat., *117,* 676–691.

Wiesenburg, D. A. and L. E. Sahl. 1994. A comparison of hydrographic conditions on the Texas-Louisiana shelf in August 1992 and 1993. The 1994 Ocean Sciences Meeting, EOS, Trans., *75,* 65.

Wiseman, W. J. Jr. and R. W. Garvine. 1995. Plumes and coastal currents near large river mouths. Estuaries, *18,* 509–517.

Wiseman, W. J. Jr. and F. J. Kelly. 1994. Salinity variability within the Louisiana coastal current during the 1982 flood season. Estuaries, *17,* 732–939.

Wright, D. G. and J. W. Loder. 1985. A depth-dependent study of the topographic rectification of tidal currents. Geophys. Astrophys. Fluid Dyn., *31,* 169–220.

Received: *27 June, 1996;* revised: *21 November, 1996.*